Optical Lattices as Quantum Simulators

Mohammad Khalifa, Dominik Koeck, Dominik Neuenfeld

***Abstract*—This report outlines the use of ultracold atoms in optical lattices to simulate quantum systems. We show how optical lattices are created and how they can be used to simulate real lattices, focusing on the case well described by the Hubbard model. We briefly comment on the rich variety of experimental applications.**

I. Introduction

Optical lattices offer a unique way to perform research on many-body systems. [1] On the one hand, they realize an accurate physical implementation of the Hubbard model. [2] Instead of atoms creating a lattice with electrons hopping from site to site, an optical lattice is created from a carefully engineered laser field. Neutral atoms can hop between adjacent potential minima, giving rise to bands just like for electrons in condensed matter systems. Optical lattices are free of vibrations and also can be made free of defects, and thus allow for a precise investigation of effects predicted using the Hubbard model. On the other hand, each of the parameters arising in the corresponding Hubbard Hamiltonian can be tuned across a wide range by adjusting the lasers used to create the lattice. Consequently, one can learn about parameter regimes which are hard to access by theoretical methods. [3] This facilitates new insights which might fuel theoretical research but also allows for a quantum simulation of the systems of interest. It is even conceivable to take advantage of the high purity of the lattice to implement quantum computing and thereby the simulation of arbitrary Hamiltonians. [4]

This report intends to give a short overview over the function and operation of optical lattices (section II) and explain how these are used to simulate a Hubbard Hamiltonian with highly tunable parameters (section III). We close with a brief description of selected experimental applications (section IV). Some mathematical details are delegated to an appendix.

II. Optical Lattices

Optical lattices use standing wave patterns of counter-propagating electromagnetic waves to create a periodic potential for ultracold atoms. This section will give a short overview of how such lattices are operated.

A. Trapping

Optical lattices rely on the *AC-Stark effect* to confine neutral atoms in their respective locations. The basis for the AC-Stark effect is a standing electromagnetic wave. The corresponding electric field induces a dipole moment in a neutral atom that usually has no permanent dipole moment and leads to an attraction or repulsion to minima or maxima of the standing wave. This effect can be modeled quantum mechanically with a simple two level atom $H_0 = \hbar\omega_0 \left|e\right\rangle \left\langle e\right| + 0 \left|g\right\rangle \left\langle g\right|$ interacting through the dipole operator $\hat{\mathbf{d}}$ with the electromagnetic field $\epsilon(\mathbf{r})$. The detailed description of this is presented in appendix A. In short, treating the interaction $H_{int} = -\hat{\mathbf{d}}\epsilon$ in second order perturbation theory after invoking the rotating wave approximation leads to an energy shift in the ground state of

$$E_g^{(2)} = \frac{\hbar|\Omega(\mathbf{r})|^2}{\delta}. \tag{1}$$

Here, $\Omega(\mathbf{r}) = \left\langle e\right| \hat{\mathbf{d}}\epsilon(\mathbf{r}) \left|g\right\rangle /\hbar = \mathbf{d_{eg}}\epsilon(\mathbf{r})/\hbar$ is the Rabi frequency and $\delta = \omega - \omega_0$ is the detuning between the two-level atom's transition frequency ω_0 and the light frequency ω. Using red detuned light with a frequency ω smaller than ω_0 leads to a lowering of the energy $E_g^{(2)}(\mathbf{r}) \leq 0$. Thus the atoms get trapped at the anti-nodes of the standing wave. On the other hand, blue detuned light $\delta > 0$ yields a positive energy correction to the ground state energy and therefore leads to a repulsion from anti-nodes. Using laser light with a frequency close to the internal transition frequency leads to a small detuning δ and therefore a large energy correction.

For a standing wave pattern of two counter-propagating electromagnetic waves $\epsilon(\mathbf{r}) = \epsilon_0(e^{i\mathbf{kr}} + e^{-i\mathbf{kr}})$, each with amplitude ϵ_0, the ground state energy correction is a periodically modulated function of $\mathbf{r}$, which results in a potential

$$V_g(\mathbf{r}) = \frac{4|\mathbf{d_{eg}}|^2 I}{\hbar\delta}\cos^2(\mathbf{kr}). \tag{2}$$

The potential depth V_g is linearly proportional to the laser intensity $I \propto \boldsymbol{\epsilon_0^2}$ and also depends on the atomic dipole moment $\mathbf{d_{eg}}$. This and the simple dependence of the lattice constant on the used laser frequency give a wide range for manipulating the optical lattice in a desired form. A simple three dimensional cubic lattice can be created by superimposing three orthogonal standing wave patterns with equal intensities I. To eliminate interference terms we may choose three orthogonal, linear polarizations $\epsilon_\mathbf{i} \cdot \epsilon_\mathbf{j} = I\delta_{ij}$ and obtain

$$V_{\text{cubic}}(\mathbf{r}) \propto I\left(\cos^2(kx) + \cos^2(ky) + \cos^2(kz)\right). \tag{3}$$

B. Lattice geometries

We can obtain the desired lattice geometries by interfering two or more laser beams. Figure 1 shows how to create one, two or three-dimensional lattices by just adding pairs of laser beams. By adjusting the laser intensity, effectively one or two-dimensional lattices can be created, as indicated by red arrow in figure 1. The details are discussed in section III-B.

Figure 2 shows how to create all five possible Bravais lattices in two dimensions. Since Bravais lattices form a complete set of possible lattice geometries, basically any lattice type in 2D can be realized. This is simply done by interfering three

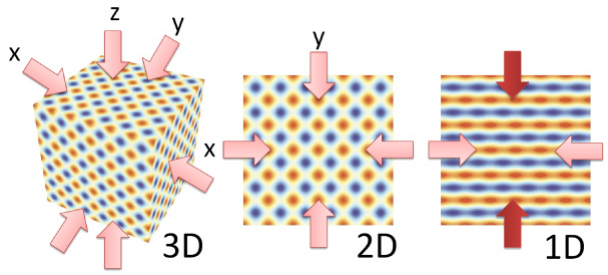

Fig. 1. Realization of different dimensions in optical lattices. The potential depth is shown in false color. Higher intensity for the Z (Z and Y) direction can be used to effectively create a 2D (1D) lattice. Figure taken from [5].

laser beams in the same plane with appropriate angles. As shown in figure 2(f) compared to 2(b), the lattice constant can also be changed by adding another laser beam. Interfering laser beams with different wavelengths leads to a beating pattern. With this beating pattern we can simulate superlattice structures [1]. Spin dependent lattices can also be realized [6]. Here, the use of circularly polarized light leads to a trapping potential that depends on the spin state of the trapped atom.

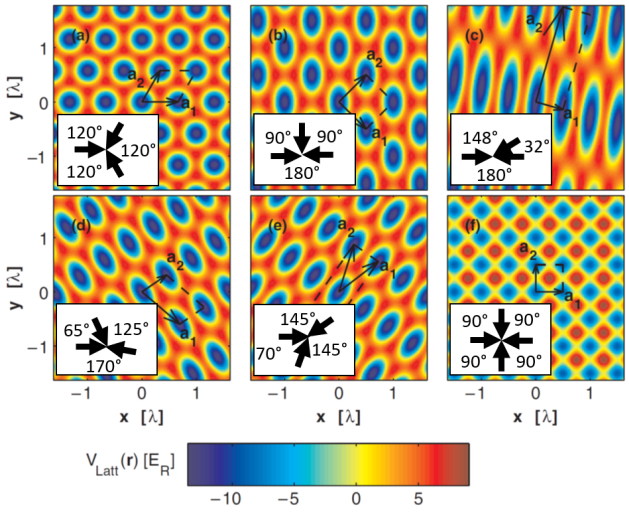

Fig. 2. The realization of all five Bravais lattices in 2D with three laser beams. (a) Hexagonal lattice, (b) square lattice, (c) rectangular lattice, (d) oblique lattice, (e) centered rectangular lattice. (f) shows a square lattice realized with four laser beams. (f) has a different lattice constant than (b). The insets show the directions of the laser beams needed to create these optical lattices. This figure was modified from Blakie and Clark [7].

C. Laser Cooling

Cooling is necessary in optical lattices in order to drive the atoms to their lowest vibrational states and keep them confined in the potential wells. The lattice barrier height is typically in the range of hundreds of micro-Kelvin, so atoms should be cooled down to temperatures of a few micro-Kelvins.

1) Doppler Cooling: The most prominent method for cooling atoms is Doppler cooling. [8] Here, the laser frequency is selected to be slightly below some internal transition frequency for the atoms required to be cooled. The atoms moving fast towards the laser source encounter photons in resonance with their internal transition due to the Doppler effect. When an atom absorbs one of these photons, its momentum decreases by the photon's momentum, because they are moving in opposite direction. The excited atom then emits a photon spontaneously in a random direction. Its momentum changes by the amount of the emitted photon's momentum although in opposite direction (*recoil momentum*). Since all the photon absorption processes are in the same direction, while the photon emission processes are in random directions, the overall effect is a decrease in the momentum and kinetic energy of the atom. By applying a laser from the opposite direction, atoms moving in either direction are slowed down resulting in an overall cooling effect for the system. Cooling takes place as long as the average momentum of the atoms is higher than the recoil momentum. When the system reaches this limit, the cooling stops and the temperature saturates at a certain value called $T_{Doppler}$ which is typically around 100 μK. [9]

2) Sub-Doppler Cooling: Cooling to temperatures even below $T_{Doppler}$ can be achieved by using other techniques such as *Sideband Cooling*. [10] There, the atoms are trapped in an optical lattice potential that is deep enough to be modeled as a harmonic potential. The atomic states can be represented by $|a, m\rangle$, where a is the internal electronic state of the atom which we assume to be either ground (g) or excited (e), and m is the harmonic oscillator vibrational state of the atom ($m = 0, 1, 2...$). If the optical lattice laser frequency is chosen to be $\omega = \omega_0 - \omega_{HO}$, where ω_0 is the internal electronic transition frequency between the states g and e while ω_{HO} is the harmonic oscillation frequency in the lattice potential, then an atom in the state $|g, n\rangle$ absorbs a photon and undergoes a transition to the state $|e, n-1\rangle$. Subsequently, the atom emits a photon spontaneously to relax to its electronic ground state $|g, n-1\rangle$. By repeating these two transitions ($|g, n\rangle \Rightarrow |e, n-1\rangle \Rightarrow |g, n-1\rangle$) the atom is cooled to its vibrational ground state $|g, 0\rangle$.

D. Loading Schemes

In order to prepare an optical lattice that exhibits interesting physics, it should be loaded with relatively high atomic density of about one atom per lattice site.

1) Adiabatic Loading: Turning on the optical lattice lasers on a free atomic gas directly will not get the atoms trapped in the lattice, because their kinetic energies are higher than the lattice potential depth. Instead, this process should be done adiabatically on a pre-cooled atomic system. Typically, atoms are loaded from a magnetic or a magneto-optic trap by turning on the optical lattice lasers slowly to superimpose its potential over the trap's potential. For instance, a Bose Einstein Condensate (BEC) can be first prepared in a magnetic trap, then loaded adiabatically to the optical lattice. [11] Initially, there will be many atoms per lattice site due to the high atomic density in the loading trap, but as the optical lattice depth increases, the atoms will undergo light-assisted collisions which increase their kinetic energy and get most of them lost. At the end, each lattice site will contain up to two atoms. The loading trap is then turned off and cooling laser beams are turned on to further cool down the optically trapped atoms to a few micro-Kelvins.

2) Irreversible loading schemes: In this set of methods, the optical lattice is turned on in an ultracold degenerate gas. The atoms start occupying the first Bloch band of the lattice. Then, they spontaneously emit phonons into the background superfluid and decay to the lowest Bloch band. The on-site repulsion in this case prevents more than one atom from occupying the same lattice site. This method can also be used to increase the filling percentage of an existing optical lattice or to cool the atoms already stored in it without affecting their internal states [12], which represents an advantage over the adiabatic loading technique.

E. Imaging techniques

To extract quantities of interest from the system, such as band occupation density, imaging techniques are used. An often employed method is *time of flight expansion imaging* in which the lattice potential is turned off and the momentum distribution of particles in the lattice is turned into a free particle momentum distribution. The system is then allowed to expand before it is illuminated by a laser tuned to the atoms' resonance frequencies to measure their location using absorption imaging: A CCD sensor captures the light which passed the atoms and their position will be visible as dark spots on the image, since the laser light was absorbed. Depending on how fast the potential is ramped down different measurements can be done. [1], [13]

1) Sudden release: The lattice lasers are turned off immediately and the particles which were located in a superposition of localized orbitals evolve in time with the free Hamiltonian. We derive in appendix B that the number density after a time t has passed is given by

$$\langle n(\mathbf{x},t)\rangle = \left(\frac{m}{\hbar t}\right)^3 \left|\tilde{w}\left(\frac{m\mathbf{x}}{\hbar t}\right)\right|^2 \mathcal{G}\left(\frac{m\mathbf{x}}{\hbar t}\right), \tag{4}$$

i.e. it is given by the Fourier transformation of the Wannier orbital multiplied by the two particle coherence function $\mathcal{G}(k)$,

$$\mathcal{G}(\mathbf{k}) = \sum_{\mathbf{R}\mathbf{R}'} e^{-i\mathbf{k}(\mathbf{R}-\mathbf{R}')}\langle a^\dagger_{\mathbf{R}} a_{\mathbf{R}'}\rangle. \tag{5}$$

This method is useful to establish the presence or absence of long range coherence, c.f. the experiment discussed in section IV-A. There, in the case of a Bose-Einstein condensate, $\langle a^\dagger_{\mathbf{R}} a_{\mathbf{R}'}\rangle$ is roughly constant at large $|\mathbf{R}-\mathbf{R}'|$, and $\mathcal{G}$ gives a standing wave interference pattern. On the other hand, if no long range coherence is present no interference is visible.

2) Adiabatic release: Turning off the lattice adiabatically allows to map out the occupancy numbers of different bands. The lattice lasers are turned off slow enough such that the particles in the lattice stay in their band. When the lasers are completely ramped down, a particle with momentum p in the nth band is mapped to a free particle of momentum of $\mathbf{p} + n\hbar\mathbf{k}$, where $\mathbf{k}$ is the size of the Brillouin zone. Thus every band gets mapped to a specific momentum range. Using absorption imaging to measure the momentum distribution, the occupancy of bands can be reconstructed. This technique is used for example in the investigation of Dirac points in artificial graphene. [14]

III. Simulating the Hubbard Hamiltonian

For strong enough potentials, the cold atoms captured in an optical lattice get localized in Wannier orbitals $w(\mathbf{x})$ around the potential minima. They can tunnel between different lattice sites. The nearest neighbor hopping and on-site interaction approximations are reasonable as long as the lattice depth $V_0 > 5E_R$, where $E_R = \hbar k/2m$ is the recoil energy. This behavior is captured by the *Hubbard Hamiltonian*. The corresponding Hamiltonian for a fermionic gas in an optical lattice is given by [2], [3],

$$H = \sum_{i,\sigma} \epsilon_i \hat{n}_{i,\sigma} - t \sum_{\langle i,j\rangle,\sigma} (\hat{c}^\dagger_{i,\sigma}\hat{c}_{j,\sigma} + \text{h.c.}) + U\sum_i n_{i,\uparrow}n_{i,\downarrow}. \tag{6}$$

The equivalent expression – the *Bose-Hubbard Hamiltonian* – for a bosonic gas is given by

$$H = \sum_i \epsilon_i \hat{n}_i - t\sum_{\langle i,j\rangle}(\hat{b}^\dagger_i \hat{b}_j + \text{h.c.}) + \frac{1}{2}U\sum_i \hat{n}_i(\hat{n}_i - 1). \tag{7}$$

In both cases ϵ_i, t and U are, respectively, the energy offset of each lattice site, the nearest neighbor hopping parameter and the on-site repulsion between two atoms. Each of these parameters is highly tunable and thus allows for the simulation of a variety of different systems.

A. Tuning the lattice site energy offset

In order to tune the energy offset ϵ_i one operates additional lasers at a larger wavelength than the lasers which create the lattice. These additional lasers create an external, slowly varying potential such that the ϵ_i are given by

$$\epsilon_i = \int d^3\mathbf{x} V_e(\mathbf{x}_i)|w(\mathbf{x}-\mathbf{x}_i)|^2 \approx V_e(\mathbf{x}_i) \tag{8}$$

An external, slowly varying potential is not always wanted, but sometimes needed for practical reasons. It can result in multiple phases in the optical lattice, e.g. one can have one phase in the center and another phase towards the boundary where $V_e(\mathbf{x})$ changes its value significantly. The offset-energy can be used to study disordered systems. To this end an additional standing light wave with wavelength λ' much larger than the one of the lattice λ is added to the optical lattice with an angle $\alpha \ll 1$ with respect to the lattice axes. This creates a spatially periodic potential with periodicity $l = \lambda'\sin(\alpha)/2$ and adds an energy offset ϵ_i that is proportional to $\cos(x_i/l)$. Adding more laser beams with different periodicities and $l_n \gg \lambda$ allows the site offset energy to be (quasi) random, realizing a disordered system. [15]

B. Tuning the hopping term

Atoms confined in an optical lattice can tunnel between lattice sites which is represented in the Hubbard Hamiltonian by the hopping term with coefficient

$$t = -\int d^3\mathbf{x} w^*(\mathbf{x}-\mathbf{R}_i)\left[\frac{-\hbar^2}{2m}\nabla^2 + V(\mathbf{x})\right] w(\mathbf{x}-\mathbf{R}_j) \tag{9}$$

taken between neighboring sites at $\mathbf{R}_i$ and $\mathbf{R}_j$. The tunneling probability between two neighboring sites is a function of the potential and depends exponentially on the width of the potential barrier, i.e. the lattice constant, and its height. During operation it is impractical to change the lattice constant and one therefore changes the tunneling probability by tuning the height of the potential. From equation (2) we can see that the lattice depth V_0 is proportional to the laser intensity times the atomic polarizability.

As mentioned in section II-B one can make the lattice barrier practically impenetrable in certain directions and realize genuine arrays of 1D and 2D lattices by ramping up the laser to a large enough intensity. Typically, the lower bound on the lattice depth is given by the requirement that the Hubbard-Hamiltonian is still a good approximation. However, in practice this limit is oftentimes fallen short of and numerical simulations must be employed.

C. Tuning on-site interactions

The contribution to the on-site interaction is dominated by scattering of particles in the same potential well and the coefficient U in the Hubbard Hamiltonian is

$$U = g \int d^3\mathbf{x} |w(\mathbf{x})|^4. \tag{10}$$

It is approximately given by the overlap of the wave function of two atoms in the same Wannier orbital $w(\mathbf{x})$ times a coupling constant $g = 4\pi a/m$, where a is the scattering length and m is the atomic mass. In order to dynamically adjust the on-site scattering amplitude U, Feshbach resonances can be employed to change the scattering length a within a wide range of positive and negative values so that it is possible to realize both, on-site repulsion and on-site attraction.

1) Feshbach Resonances: Feshbach resonances exploit resonant scattering of atoms. As a simple example consider a two-channel Hamiltonian $\mathcal{H}$ with one open and one closed channel. This means that $\mathcal{H}$ has one inaccessible (bound) eigenstate $|C\rangle = \psi(r)|c\rangle$ with energy E_c. The state $|c\rangle$ labels the channel, which is closed in this case. In addition to this bound state, there is a continuum of eigenstates $|E\rangle = \phi(r, E)|bg\rangle$, where $|bg\rangle$ is the open background scattering channel. The wave functions $\psi(r)$ and $\phi(r, E)$ are eigenfunctions of the Hamiltonian with the potentials V_c and V_{bg} given in figure 3.

If the Hamiltonian contains a small mixing term $\propto |c\rangle\langle bg| + h.c.$ true eigenstates are mixtures of the ones given above. If the atoms in the trap have different magnetic moments, an external magnetic field can be used to tune E_c to lie above or below E. If E is close to E_c the two channels strongly mix. This changes the scattering length. For these *magnetically tuned* Feshbach resonances, the scattering length is given as a function of an external magnetic field B as

$$a = a_{bg}\left(1 - \frac{\Delta}{B - B_0}\right), \tag{11}$$

where a_{bg} is the scattering length associated with V_{bg}, Δ is called *scattering-width* and B_0 is called the *resonance position*.

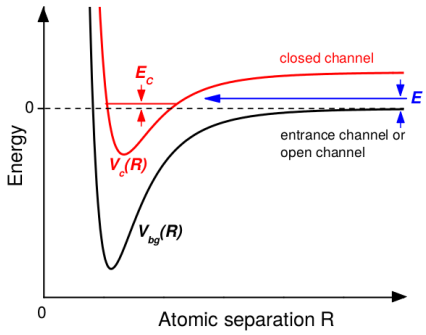

Fig. 3. The two channels of a Feshbach resonance. The red curve corresponds to the closed channel $|c\rangle$, while the black curve corresponds to the open channel $|bg\rangle$. The potential curves are given in the center of mass frame. Figure taken from [16].

Another method that can be employed to control the scattering length is *optical Feshbach resonances*. There, instead of using a magnetic field to tune the energy levels of a system, one tunes an external laser so that atoms can almost access a vibrational mode. [16]

The on-site repulsion U also depends on the lattice depth V_0 as $V_0^{(D/4)}$ where D is the lattice dimensionality, since the form of the Wannier orbitals depends on the lattice height.

IV. Experiments

In the following we will present a selection of experimental applications for optical lattices.

A. Mott-Superfluid transition

A simple cubic lattice like the one in equation 3 has been used [17] to observe phase transitions of bosonic ^{87}Rb atoms from a Mott-insulating state to a superfluid state. Those two states are two possible phases predicted by the Bose-Hubbard model and are shown in the phase diagram in figure 4.

1) Superfluid phase: The superfluid state results from the limit $U \ll t$, when a small potential depth V_0, achieved with a low laser intensity, is used to create the optical lattice. The number of lattice sites will be denoted as N_L. Below the critical temperature for Bose-Einstein condensation, all N atoms condense in the same lowest energy Bloch state

$$|GS\rangle_{U\ll t} = \frac{1}{\sqrt{N!}}\left(\hat{b}^\dagger_{k=0}\right)^N |0\rangle = \frac{1}{\sqrt{N!}}\left(\frac{1}{\sqrt{N_L}}\sum_{i=1}^{N_L}\hat{b}^\dagger_i\right)^N |0\rangle . \tag{12}$$

This is a superfluid and can be described by a macroscopic wavefunction with long-range phase coherence throughout the lattice [18].

2) Mott insulating phase: If we increase the potential depth by increasing the laser intensity, we can simulate the limit $U \gg t$, which will give rise to a Mott insulating phase. For an integer ratio of atoms to lattice sites $n = \frac{N}{N_L}$, in the ground state each lattice site is occupied with exactly n atoms. For instance for $n = 1$ we have

$$|GS\rangle_{U\gg t} = \left(\prod_{i=1}^{N_L}\hat{b}^\dagger_i\right)|0\rangle . \tag{13}$$

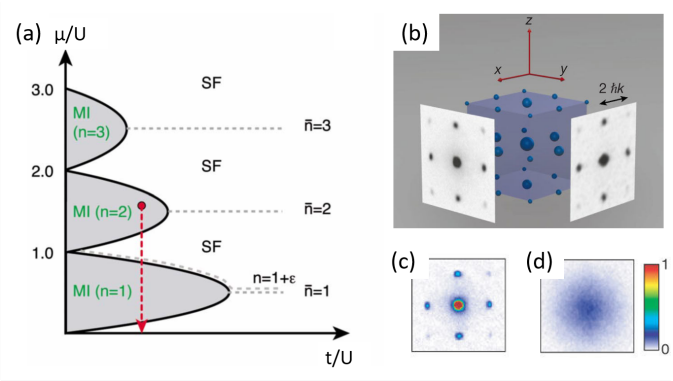

Fig. 4. (a) Zero-temperature phase diagram of the Bose-Hubbard model. Each of the lobes corresponds to an integer number $n = 1, 2, 3$ of atoms fixed at each site. Additional atoms $n = 1 + \epsilon$ on top of integer average numbers remain in the superfluid regime (see dashed line). (b) shows an illustration how a system characterization is performed. Cold atoms are illuminated after a sudden removal of the lattice potential and the absorption images are measured using CCD-cameras. This method is explained in section II-E. (c) The absorption intensity after 15 ms of free flight for a superfluid state for a $V_g = 3E_R$ deep lattice potential. The resulting interference pattern is due to the macroscopic coherence present in the superfluid state of the atoms. (d) Absorption image after 15 ms for a Mott state. The lattice depth is $V_g = 20E_R$. The uniform distribution shows, that no large scale coherence is present. These figures have been taken from [1] and [17] in a modified form.

In this state each atom is fixed to its lattice site making it immobile. The Mott state is characterized by being incompressible $\frac{\partial n}{\partial \mu} = 0$ under change of the chemical potential μ [1]. We therefore find lobes of constant occupation numbers as shown in figure 4(a). A transition can simply be done by changing the lattice potential depth, hence changing the ratio t/U. A comparable experiment on a real material has been done for NiO [19], where the transition from a Mott-insulating to a metal phase was observed. Since in a real material we have electrons which are fermions, the limit $U \ll t$ gives a metal phase instead of a condensation into a superfluid. Trying to decrease the on-site repulsion U to leave the Mott-insulating state for a real material like NiO, requires high pressures in the order of 240 GPa [19].

B. Quantum Computing

Ultracold atoms in optical lattices have many features that make them a good platform for quantum information processing, such as long coherence time, scalability, and reliable control and readout of qubits. [20] Each individual atom trapped at a certain lattice site represents a well defined qubit. There are many techniques to implement quantum computing with these atomic qubits. Here, we briefly mention only two examples of how to realize single and double qubit operations in optical lattices.

1) Single Qubit Operations: An optical lattice is used in the Mott phase for quantum computing. The logical states $|0\rangle$ and $|1\rangle$ of the qubit are defined as two hyperfine magnetic states, for example $m_F = 1$ and $m_F = -1$, with energy shift $\hbar\omega_0$ between them. By applying a resonant electromagnetic pulse, an arbitrary superposition $\alpha|0\rangle + \beta|1\rangle$ can be realized, where α and β are controlled by the duration of the pulse. In order to manipulate a single qubit without affecting the surrounding qubits, techniques can be used to change the transition frequency of this qubit with respect to the other ones in the lattice [21] (see Appendix C for details).

2) Double Qubit Operations: One of the methods to entangle two atomic qubits in an optical lattice is by collisional interaction. [22] Consider two atoms in neighboring lattice sites (j and $j+1$) each in the maximum superposition state, i.e. their total state is given by $|\Psi\rangle = (|0\rangle_j + |1\rangle_j)(|0\rangle_{j+1} + |1\rangle_{j+1})/2$. Now, assume the polarization of the optical lattice laser is slowly changed. Since different magnetic states interact differently to a circularly polarized field, the two states of the atoms will have two spatially different potential minima. For instance, the $|0\rangle$ state moves to the left and the $|1\rangle$ state moves to the right to be at their new potential minima, such that the total state becomes $|\Psi\rangle = (|0\rangle_l|0\rangle_{l+1} + |0\rangle_l|1\rangle_{l+2} + |1\rangle_{l+1}|0\rangle_{l+1} + |1\rangle_{l+1} + |1\rangle_{l+2})/2$, where the position l is between positions $j-1$ and j. From the third term in this expression, the state $|1\rangle$ of the first atom and the state $|0\rangle$ of the second atom are on the same site and, therefore, they undergo an on-site interaction U_{01}. After time t_{int}, a phase shift $\phi = t_{int}U_{01}/\hbar$ has accumulated and the total state turns into $|\Psi\rangle = (|0\rangle_l|0\rangle_{l+1} + |0\rangle_l|1\rangle_{l+2} + e^{-i\phi}|1\rangle_{l+1}|0\rangle_{l+1} + |1\rangle_{l+1} + |1\rangle_{l+2})/2$. By returning the lasers to their linear polarization state and applying a resonant electromagnetic pulse to the qubits, the system state finally becomes $|\Psi\rangle = [(1 + e^{-i\phi})|1\rangle_j|1\rangle_{j+1} + (1 - e^{-i\phi})|B\rangle]/2$, where $|B\rangle$ is a maximum entangled state given by $|B\rangle = |0\rangle_j|-\rangle_{j+1} + |1\rangle_j|+\rangle_{j+1}$. Full entanglement between the two qubits is achieved by controlling the time t_{int} such that $\phi = \pi$.

3) Universal Quantum Simulation: With the single and double qubit operations, a quantum computing system can simulate any other many-body system whose Hamiltonian consists of one-particle and two-particle terms. The idea here is to decompose any Hamiltonian H into small Hamiltonians H_j, each of which acts on a small constant subspace, so that $H = \sum_j H_j$. Then, the system evolution e^{-iHt} can be represented as a series of short evolutions e^{-iH_jt} according to Trotter formula $e^{-iHt} = \lim_{m\to\infty}(e^{-iH_1t/m}e^{-iH_2t/m}e^{-iH_3t/m}...)^m$. Trapped atoms in optical lattices provide an example of such quantum system that is capable of doing this series of single and double qubit operations with high fidelity. [15]

V. Conclusions

We gave a brief summary of the use of optical lattices to simulate quantum systems and a summary of selected applications. It should go without saying that, beyond what was covered in this this report, there are many more interesting facets to this topic. For example, there are a plenty advanced experimental techniques, such as the introduction of lattice impurities [15] or frustrated systems [23]. Also other methods are available for imaging. [24], [25] Many exciting experimental applications have not been touched upon. Good places to start reading are the reviews referenced below. [1], [3], [13], [26]

REFERENCES

[1] Immanuel Bloch, Jean Dalibard, and Wilhelm Zwerger. Many-body physics with ultracold gases. *Reviews of Modern Physics*, 80(3):885–964, 2008.

[2] J Hubbard. Electron Correlations in Narrow Energy Bands. *Proceedings of the Royal Society A: Mathematical, Physical and Engineering Sciences*, 276(1365):238–257, 1963.

[3] Tilman Esslinger. Fermi-Hubbard Physics with Atoms in an Optical Lattice. *Annual Review of Condensed Matter Physics*, 1(1):129–152, 2010.

[4] Andrew J. Daley. Quantum computing and quantum simulation with group-II atoms. *Quantum Information Processing*, 10(6):865–884, 2011.

[5] D C Mckay and B Demarco. Cooling in strongly correlated optical lattices: prospects and challenges. *Reports on Progress in Physics Rep. Prog. Phys*, 74:54401–29, 2011.

[6] D. McKay and B Demarco. Thermometry with spin-dependent lattices. *New Journal of Physics*, 12(12), 2010.

[7] P Blair Blakie and Charles W Clark. Wannier states and Bose-Hubbard parameters for 2D optical lattices. In *Journal of Physics B: Atomic, Molecular and Optical Physics*, volume 37, pages 1391–1404, 2004.

[8] T. W. Hänsch and A. L. Schawlow. Cooling of gases by laser radiation. *Optics Communications*, 13(1):68–69, 1975.

[9] Rudolf Grimm, Matthias Weidemüller, and Y Ovchinnikov. Optical dipole trap for neutral atoms. *Adv. At. Mol. Opt. Phys.*, 42:95, 2000.

[10] Andrew J. Kerman, Vladan Vuletić, Cheng Chin, and Steven Chu. Beyond Optical Molasses: 3D Raman Sideband Cooling of Atomic Cesium to High Phase-Space Density. *Physical Review Letters*, 2000.

[11] S. Peil, J. V. Porto, B. Laburthe Tolra, J. M. Obrecht, B. E. King, M. Subbotin, S. L. Rolston, and W. D. Phillips. Patterned loading of a Bose-Einstein condensate into an optical lattice. *Physical Review A*, 2003.

[12] A. J. Daley, P. O. Fedichev, and P. Zoller. Single-atom cooling by superfluid immersion: A nondestructive method for qubits. *Physical Review A*, 69(2):022306, 2004.

[13] Bertrand Halperin and Alexander Sevrin. Proceedings of the 24th Solvay Conference on Physics. In Bertrand Halperin and Alexander Sevrin, editors, *Quantum Theory of Condensed Matter*, Solvay, 2010. World Scientific.

[14] Leticia Tarruell, Daniel Greif, Thomas Uehlinger, Gregor Jotzu, and Tilman Esslinger. Creating, moving and merging Dirac points with a Fermi gas in a tunable honeycomb lattice. *Nature*, 483(7389):302–305, 2012.

[15] Dieter Jaksch and P Zoller. The cold atom Hubbard toolbox, 2005.

[16] Cheng Chin, Rudolf Grimm, Paul Julienne, and Eite Tiesinga. Feshbach resonances in ultracold gases. *Reviews of Modern Physics*, 82(2):1225–1286, 2010.

[17] Markus Greiner, Olaf Mandel, Tilman Esslinger, Theodor W Ha, Nsch, and Immanuel Bloch. Quantum phase transition from a superuid to a Mott insulator in a gas of ultracold atoms. *NATURE*, 415(3), 2002.

[18] T. Csorgo. Coherent states of the creation operator from fully developed Bose-Einstein condensates. 3 1999.

[19] Alexander G. Gavriliuk, Ivan A. Trojan, and Viktor V. Struzhkin. Insulator-Metal Transition in Highly Compressed NiO. *Physical Review Letters*, 109(8):086402, 8 2012.

[20] Immanuel Bloch. Quantum coherence and entanglement with ultracold atoms in optical lattices. *Nature*, 453(7198):1016–1022, 2008.

[21] Yang Wang, Xianli Zhang, Theodore A. Corcovilos, Aishwarya Kumar, and David S. Weiss. Coherent Addressing of Individual Neutral Atoms in a 3D Optical Lattice. *Physical Review Letters*, 115(4), 2015.

[22] Olaf Mandel, Markus Greiner, Artur Widera, and Tim Rom. Controlled collisions for multi- particle entanglement of optically trapped atoms. *Nature*, 425(6961):937–940, 2003.

[23] Maciej Lewenstein, Anna Sanpera, Veronica Ahufinger, Bogdan Damski, Aditi Sen, and Ujjwal Sen. Ultracold atomic gases in optical lattices: Mimicking condensed matter physics and beyond. *Advances in Physics*, 56(2):243–379, 2007.

[24] Maxwell F. Parsons, Florian Huber, Anton Mazurenko, Christie S. Chiu, Widagdo Setiawan, Katherine Wooley-Brown, Sebastian Blatt, and Markus Greiner. Site-Resolved imaging of fermionic li 6 in an optical lattice. *Physical Review Letters*, 114(21):1–5, 2015.

[25] Karl D. Nelson, Xiao Li, and David S. Weiss. Imaging single atoms in a three-dimensional array. *Nature Physics*, 3(8):556–560, 2007.

[26] Dieter Jaksch and P. Zoller. The cold atom Hubbard toolbox. *Annals of Physics*, 315(1):52–79, 2005.

APPENDIX A
TRAPPING, THE AC STARK EFFECT

Consider a two level atom with a transition frequency $\omega_0 = \frac{E_e - 0}{\hbar}$ in a classical electromagnetic field $\mathbf{E}(x,t) = \epsilon(\mathbf{x})e^{-i\omega t} + \epsilon^*(\mathbf{x})e^{i\omega t}$. The Hamiltonian of the atom in that field can than be expressed in the basis of the excited $|e\rangle$ and the ground state $|g\rangle$:

$$H = H_0 + H' = H_0 - \hat{\mathbf{d}}\mathbf{E} \tag{14}$$

$$= \hbar\omega_0 |e\rangle\langle e| - \sum_{\alpha,\alpha'=g,e} |\alpha\rangle\langle\alpha|\hat{\mathbf{d}}|\alpha'\rangle\langle\alpha'|\mathbf{E} \tag{15}$$

Because a single atom doesn't have a permanent dipole, the dipole matrix elements are nonzero only for the off-diagonal elements $\mathbf{d_{eg}} = \langle e|\hat{\mathbf{d}}|g\rangle$ and $\mathbf{d^*_{eg}} = \langle g|\hat{\mathbf{d}}|e\rangle$. Transforming to the rotating frame picture with $U = e^{-iH_0/\hbar \cdot t}$ and defining the Rabi frequency $\Omega = \mathbf{d_{eg}}\epsilon(\mathbf{x})/\hbar$, we get

$$U^\dagger H' U = -\hbar\Omega e^{-i(\omega-\omega_0)t}|e\rangle\langle g| - \hbar\Omega^* e^{i(\omega-\omega_0)t}|g\rangle\langle e|. \tag{16}$$

Here we already applied the so called rotating wave approximation, where we neglect fast oscillating terms $\omega + \omega_0$. This is justified if the light frequency ω is close to the transition resonance frequency ω_0. After transforming back in the Schrödinger picture and inserting in the full Hamiltonian, we get:

$$H_{RWA} = H_0 - \hbar\Omega e^{-i\omega t}|e\rangle\langle g| - \hbar\Omega^* e^{i\omega t}|g\rangle\langle e|. \tag{17}$$

We can treat the effects of the light field as a perturbation in second order perturbation theory and get an energy correction

$$E_g^{(2)} = \frac{|\langle g|H'|e\rangle|^2}{E_g - E_e} = \frac{\hbar|\Omega(x)|^2}{\delta} \tag{18}$$

for the ground state, and $E_e^{(2)} = -\frac{\hbar|\Omega(x)|^2}{\delta}$ for the excited state. We have $E_g - E_e = \hbar\omega n - (\hbar\omega_0 + \hbar\omega(n-1)) = \hbar(\omega - \omega_0) = \hbar\delta$ because the true ground state energy is that of n photons and the excited state energy is the energy of the excited state plus the energy of $n-1$ photons, after one photon has been absorbed. Assuming a standing wave pattern of two counter-propagating electromagnetic waves $\epsilon_0(x) = \epsilon_0(e^{i\mathbf{kr}} + e^{-i\mathbf{kr}})$, each with amplitude ϵ_0, gives the desired lattice potential as the ground state energy correction:

$$V_g(x) = \frac{|\mathbf{d_{eg}}|^2|2\epsilon_\mathbf{0}|^2}{\hbar\delta}\cos^2(\mathbf{kr}) = \frac{4|\mathbf{d_{eg}}|^2 I}{\hbar\delta}\cos^2(\mathbf{kr}). \tag{19}$$

APPENDIX B
IMAGING WITH SUDDEN RELEASE

The number density of particles is given by the absolute square of the wave function. In terms of Wannier functions $w(x-R)$ and creation/annihilation operators which create states in a Wannier orbital at site R, the creation/annihilation operators for particles at position x are given by

$$a_\mathbf{x} = \sum_\mathbf{R} w(\mathbf{x}-\mathbf{R})a_\mathbf{R} \quad a^\dagger_\mathbf{x} = \sum_\mathbf{R} w^*(\mathbf{x}-\mathbf{R})a^\dagger_\mathbf{R}. \tag{20}$$

The expected number density then becomes

$$\langle n(\mathbf{x})\rangle = \langle a^\dagger_{\mathbf{x}} a_{\mathbf{x}}\rangle = \iint d^3\mathbf{k} d^3\mathbf{k}' e^{i(\mathbf{k}-\mathbf{k}')\mathbf{x}} \tilde{w}(\mathbf{k})\tilde{w}^*(\mathbf{k}')\mathcal{G}(\mathbf{k},\mathbf{k}'), \tag{21}$$

where we have defined the two site correlation function

$$\mathcal{G}(\mathbf{k},\mathbf{k}') = \sum_{\mathbf{R}\mathbf{R}'} e^{-i\mathbf{k}\mathbf{R}+i\mathbf{k}'\mathbf{R}'}\langle a^\dagger_{\mathbf{R}} a_{\mathbf{R}'}\rangle. \tag{22}$$

After free evolution for a time t, the kth mode acquires a phase of $\exp(-i\frac{\hbar\mathbf{k}^2}{2m}t)$ and equation (21) becomes

$$\langle n(\mathbf{x},t)\rangle = \iint d^3\mathbf{k} d^3\mathbf{k}' e^{i(\mathbf{k}-\mathbf{k}')\mathbf{x}} e^{-i\frac{\hbar(\mathbf{k}^2-\mathbf{k}'^2)}{2m}} \cdot \tilde{w}(\mathbf{k})\tilde{w}^*(\mathbf{k}')\mathcal{G}(\mathbf{k},\mathbf{k}'). \tag{23}$$

We can now shift $\mathbf{k} \to \mathbf{k} + \frac{m\mathbf{x}}{\hbar t}$ and obtain

$$\langle n(\mathbf{x},t)\rangle = \iint d^3\mathbf{k} d^3\mathbf{k}' e^{-i\frac{\hbar(\mathbf{k}^2-\mathbf{k}'^2)}{2m}} \tilde{w}\left(\mathbf{k}+\frac{m\mathbf{x}}{\hbar t}\right) \cdot \tilde{w}^*\left(\mathbf{k}'+\frac{m\mathbf{x}}{\hbar t}\right)\mathcal{G}\left(\mathbf{k}+\frac{m\mathbf{x}}{\hbar t},\mathbf{k}'+\frac{m\mathbf{x}}{\hbar t}\right) \tag{24}$$

Finally, a saddle-point approximation yields

$$\langle n(\mathbf{x},t)\rangle = \left(\frac{m}{\hbar t}\right)^3 \left|\tilde{w}\left(\frac{m\mathbf{x}}{\hbar t}\right)\right|^2 \mathcal{G}\left(\frac{m\mathbf{x}}{\hbar t}\right). \tag{25}$$

We see that the number density is basically the Fourier transformation of the Wannier orbital multiplied by an interference term which depends on the occupancy of different modes.

Appendix C
Addressing Individual Atoms

To address individual qubits in an optical lattice quantum system, two modes of operation should be defined; storage mode and computational mode. Assume that the $|0\rangle$ and $|1\rangle$ states of the qubit are the hyperfine ground sublevel states $F = 3$ and $F = 4$, with $m_F = 0$ for the storage mode ($|3,0\rangle$ and $|4,0\rangle$ are *storage basis*), and $m_F = 1$ for the computational mode ($|4,1\rangle$ and $|3,1\rangle$ are *computational basis*). All qubits are initially kept in the storage basis. When a quantum operation is required to be done on a certain qubit, only this (target) qubit is transfered from the storage to the computational basis. This is done by applying two addressing circularly polarized beams crossing at the target lattice site and a static magnetic field in their plane, as shown in figure 5(a). The role of the addressing beams is to change the resonant frequency (the internal states) of the target atom only. The role of the magnetic field is to split the magnetic internal states of the target atom to create more than one resonant frequency. Now, only the target atom has resonant transitions with ω_1 that corresponds to $|3,0\rangle \Leftrightarrow |4,1\rangle$ or $|4,0\rangle \Leftrightarrow |3,1\rangle$ transitions, and ω_2 that corresponds to $|3,1\rangle \Leftrightarrow |4,1\rangle$ transition, as illustrated in figure 5(b). Since the target atom is initially in the storage basis, then it can be transfered to the computational basis by applying a microwave pulse with frequency ω_1 on the lattice. The next step is to do the quantum operation on the target qubit in the computational basis, which can be realized by applying a second arbitrary microwave pulse with frequency ω_2 to control the superposition $\alpha|0\rangle + \beta|1\rangle$ of the qubit. Then, another microwave pulse with frequency ω_1 is applied to return the atom back to the storage basis and, finally the addressing beams and the magnetic field are turned off. [21]

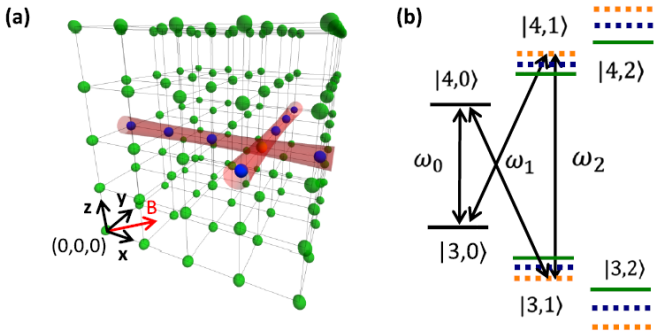

Fig. 5. (a) Addressing individual atom in a 3D optical lattice. The addressing beams cross at the target atom to change its resonance from other atoms resonance. A magnetic field is applied in the same plane to split the magnetic sublevels. (b) Atomic levels in storage and computational basis. The atom is resonant with ω_0 in storage basis, with ω_2 in computational basis and with ω_1 at the transfer between the two bases. The graph is not to scale. [21]